

## Noncollinear Surface Spin Density by Surface Reconstruction in the Alloy NiMn

C. L. Gao,<sup>1</sup> A. Ernst,<sup>1</sup> A. Winkelmann,<sup>1</sup> J. Henk,<sup>1</sup> W. Wulfhekel,<sup>1,2</sup> P. Bruno,<sup>1</sup> and J. Kirschner<sup>1</sup>

<sup>1</sup>Max-Planck-Institut für Mikrostrukturphysik, Weinberg 2, 06120 Halle, Germany

<sup>2</sup>Physikalisches Institut, Universität Karlsruhe (TH), Wolfgang-Gaede Strasse 1, 76131 Karlsruhe, Germany

(Received 13 January 2008; published 11 June 2008)

At the (001) surface of the alloy Ni<sub>50</sub>Mn<sub>50</sub>, a noncollinear spin density is observed in real space by spin-polarized scanning tunneling microscopy. The spin density of individual atoms also varies in both size and direction as a function of bias voltage, indicating a noncollinearity in the energy domain. The noncollinearity is driven by a surface reconstruction which breaks the otherwise high surface symmetry. First-principles electronic-structure calculations support the experimental observations and evidence the interplay of reconstruction and spin-orbit coupling.

DOI: [10.1103/PhysRevLett.100.237203](https://doi.org/10.1103/PhysRevLett.100.237203)

PACS numbers: 75.70.Ak, 68.37.Ef, 75.50.Ee, 75.70.Rf

Antiferromagnets in contact with ferromagnets—known as exchange-biased systems—play an important role in many magnetoelectronic devices [1]. The exchange-bias effect is due to the exchange interaction across the antiferromagnet-ferromagnet interface. Detailed understanding of the spin polarization on the atomic level of antiferromagnetic surfaces is therefore helpful in understanding exchange bias. With the development of spin-polarized scanning tunneling microscopy (Sp-STM), it became possible to study spin configurations at antiferromagnetic surfaces with atomic resolution [2]. While Sp-STM studies on antiferromagnets have been carried out predominantly on pure elements [2,3], the technologically relevant antiferromagnets are alloys (e.g., FeMn [4], IrMn [5], and NiMn [6,7]). NiMn gains special interest because of its thermal stability, corrosion resistance, and high Néel temperature (1070 K) [8].

In this joint experimental and theoretical investigation, we show by Sp-STM that the surface spin density of NiMn films is noncollinear in space and energy, contrary to expectations. The very reason for this effect is a broken surface symmetry, details of which are obtained by low-energy electron diffraction (LEED) analysis. The atomic relaxations—in interplay with spin-orbit coupling—result in a complicated, noncollinear, and energy-dependent spin polarization, as is supported by first-principles electronic-structure calculations.

Chemically ordered Ni<sub>50</sub>Mn<sub>50</sub> shows a CuAu-I face-centered tetragonal structure ( $L1_0$  with lattice constants  $a = b = 3.74$  Å and  $c = 3.52$  Å [9]). Mn and Ni atoms occupy alternating atomic sheets perpendicular to the  $c$  axis. The magnetic moments of adjacent Mn atoms ( $3.8\mu_B$ ) lie within the Mn sheets and are antiparallelly aligned while the Ni moments vanish [8], resulting in a layerwise antiferromagnetic structure along the  $a$  or the  $b$  direction, as was shown by neutron diffraction experiments. Recently, it has been reported that chemically ordered equiatomic NiMn can be grown epitaxially on Cu(001) [10]. Exchange bias was observed by depositing

Co on NiMn/Cu(001), indicating that the NiMn thin films are antiferromagnetic.

The experiments were performed in ultrahigh vacuum (base pressure  $<1 \times 10^{-10}$  mbar). Cu(001) was cleaned by cycles of Ar<sup>+</sup> sputtering and annealing to 800 K. Ni and Mn were deposited while keeping the substrate at room temperature, followed by annealing at 350 K. The NiMn composition was checked by medium-energy electron diffraction whose intensity oscillations reflect the layer-by-layer growth of Ni and NiMn on Cu(001) [10]. For the Sp-STM measurements at 300 K, a ferromagnetic CoFeSiB ring was used as a STM electrode [11]. The magnetization direction of the ring  $\vec{M}_{\text{ring}}$  is switched periodically between two stable states of opposite magnetization. Because of the tunnel magnetoresistance effect, the tunnel current between ring and sample depends on the direction of  $\vec{M}_{\text{ring}}$  with respect to the sample spin polarization. Hence, the difference of the two associated tunnel currents is proportional to the projection of the spin polarization on the ring tangential [3]. A major advantage of this method is that the ring has a well-defined direction of in-plane spin sensitivity, determined by its shape [12]. Further, the signal is of purely magnetic origin [13]. This technique is therefore well suited for investigating alloy films. A detailed description can be found elsewhere [13].

The structure of NiMn films on Cu(001) is similar to that of the respective bulk, with Ni and Mn atomic sheets oriented perpendicular to the Cu(001) surface. In this configuration, the chemical unit cell [Fig. 1(c)] naturally results in a  $c(2 \times 2)$  LEED pattern [10].

Indeed, bright dots in the atomically resolved topography obtained by STM clearly form  $c(2 \times 2)$  cells [e.g., square I with dimension  $3.6$  Å  $\times$   $3.6$  Å, Fig. 1(a)]. A careful analysis of the STM image shows, however, that the central atom in square II slightly shifts from the center towards the right-bottom corner. Further, every second bright dot appears higher (brighter) and every second dark depletion deeper (darker). Both observations are com-

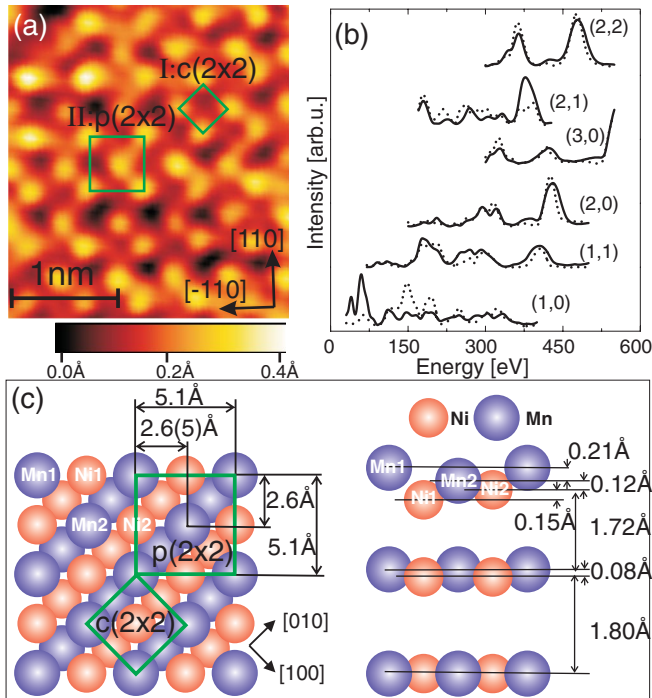


FIG. 1 (color). (a) Atom-resolved topography of 14.7 monolayers (ML) NiMn on Cu(001) taken with a W tip ( $U = 20$  mV,  $I = 3$  nA). The squares show the  $c(2 \times 2)$  chemical unit cell as well as the larger  $p(2 \times 2)$  unit cell. (b) LEED-IV curves of 12 ML NiMn films (solid curve: experimental; dotted curve: best-fit theory). (c) Geometric structure of NiMn as obtained from the LEED-IV analysis. Left: In-plane positions of atoms in the surface and subsurface layers. Note the alternating Mn and Ni sheets perpendicular to the surface. Right: Perpendicular relaxations of atoms Mn1, Mn2, Ni1, and Ni2.

patible with a larger  $p(2 \times 2)$  cell and indicate a broken  $c(2 \times 2)$  symmetry by surface reconstruction.

Because relaxations in alloys can hardly be quantified by STM, a LEED-IV analysis is performed to determine the atomic positions, using the SATLEED package [14]. Allowing only relaxations perpendicular to the surface in the outermost two layers while keeping the lateral positions as prescribed by the substrate results in a best-fit geometry with a Pendry  $R$  factor of 0.36 [Fig. 1(b)]. An error of  $\pm 0.05$  Å in the atomic positions is estimated from the variance of the  $R$  factor [15]. The outward relaxation of the Mn atoms is much larger than those of the Ni atoms [Fig. 1(c)]. As a result, bright protrusions in the STM image are identified as Mn atoms [Fig. 1(a)]. The surface atoms are deliberately separated into two groups: Mn1 and Mn2 as well as Ni1 and Ni2 which differ in their perpendicular relaxation. Considering the lateral displacement of the surface atoms, which is evident from the STM analysis, a slightly improved LEED-IV fit ( $R$  factor: 0.34) is obtained with Mn2 atoms laterally displaced off the Mn sheets [left in Fig. 1(c)]. Both the size and direction of this displacement are compatible with the STM data.

Because of the fourfold symmetry of the Cu(001) substrate, two orthogonal domains of NiMn can exist. These are distinguished by the orientations of the Mn sheets either along [100] or along [010]. In the large scale topographic image [Fig. 2(a)], atomically flat terraces and islands are observed. Indications of the direction of the Mn planes in the different domains are missing, as the topographic STM images mainly reflect the electronic differences between Ni and Mn of the top layer. On the contrary, the spin-resolved image shows two different spin patterns [marked as domains 1 and 2 in Fig. 2(b)]. Domain 1 displays a checkerboard structure whose unit cell coincides with the  $c(2 \times 2)$  chemical unit cell. Domain 2 exhibits parallel lines, the separation of which equals that of adjacent Mn sheets. Hence, one is lead to conclude that these spin patterns reflect two structural domains with orthogonal Mn sheets. Note that contrast between atomic layers is not observed, implying an in-plane compensated spin density. From the symmetry point of view, the magnetic properties of the domains are expected to be identical, but they appear differently in the spin-resolved STM image because the projections of their spin polarizations onto the spin-sensitive direction  $\vec{M}_{\text{ring}}$  of the STM differ.

Depending on the domain orientation with respect to  $\vec{M}_{\text{ring}}$ , the spin pattern is either shifted or not shifted when crossing an atomic step edge. For example, a shift of half of the  $c(2 \times 2)$  cell across the step is found, as indicated by the black line in Fig. 2(b). This allows us to determine the Mn-sheet orientations with respect to  $\vec{M}_{\text{ring}}$  if the bulk magnetic structure is assumed for the subsurface NiMn layers. As a result,  $\vec{M}_{\text{ring}}$  is parallel to the Mn sheets in domain 1 and perpendicular to Mn sheets in domain 2.

A detailed analysis reveals that the spin polarization of the tunnel current depends significantly on the bias voltage

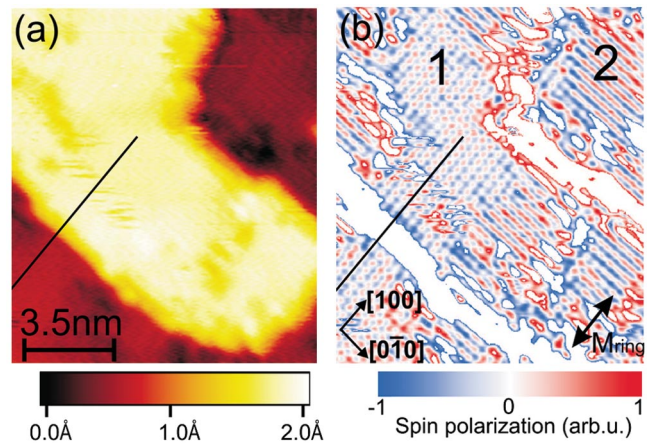


FIG. 2 (color). (a) Topography and (b) related spin signal of 12 ML NiMn/Cu(001). 1 and 2 indicate two different spin patterns. The color scale gives the relative spin polarization along  $\vec{M}_{\text{ring}}$ , with white as zero.  $\vec{M}_{\text{ring}}$  represents the spin-sensitive direction of the STM tip.  $U = 0.5$  V,  $I = 3$  nA.

(negative voltages correspond to tunneling from occupied states of the sample). For domain 1 ( $\vec{M}_{\text{ring}}$  parallel to the sheets; upper row in Fig. 3), the spin-resolved image for  $-0.1$  V shows weak contrast, evidently with  $p(2 \times 2)$  cells. This agrees with both the atom-resolved topography and the LEED-IV analysis. At positive voltages, the spin unit cell is reduced to dimension  $3.6 \text{ \AA} \times 3.6 \text{ \AA}$  and conforms with the  $c(2 \times 2)$  chemical unit cell. For domain 2 ( $\vec{M}_{\text{ring}}$  perpendicular to the sheets; center row), there is apparently no ordered feature at negative bias voltages. The spin pattern at positive voltages is characterized by parallel stripes separated by  $3.6 \text{ \AA}$ . The stripes reflect the twofold symmetry of the film due to the atomic sheets. Note that all images were taken with the same STM tip, allowing direct comparison of the orthogonal projections of the spin polarization. If the surface spin structure were collinear, i.e., the spin polarization of all individual atoms are aligned along a unique axis, the spin patterns of the two domains should be identical, except for a scale factor. Thus, the difference of the patterns at positive voltages reflects the noncollinearity of the spin polarization in real space, and the change of the spin unit cell in domain 1 from  $p(2 \times 2)$  to  $c(2 \times 2)$  indicates a change of the spin polarization direction as a function of bias voltage. The latter can be viewed as noncollinearity of the spin polarization in the energy domain (in the collinear case, only the size of spin polarization may change with the energy of the electrons).

The two kinds of noncollinearity (in real space and in energy) are easily identified by combining two spin pat-

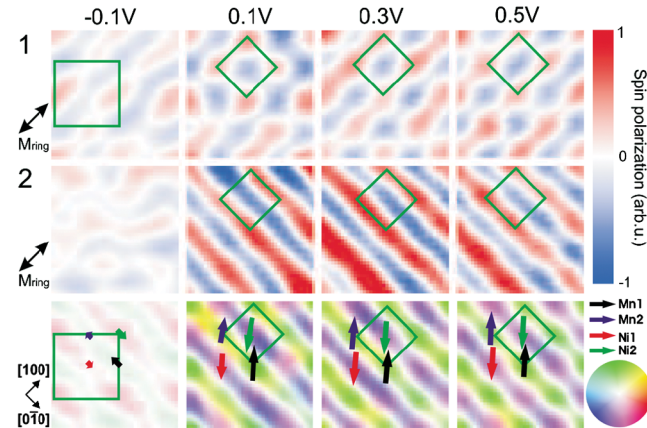


FIG. 3 (color). Spin-resolved STM images of NiMn for selected bias voltages ( $-0.1$  to  $0.5$  V, as indicated on the top) at domain 1 (top row) and domain 2 (center row). The images of dimension  $1 \text{ nm} \times 1 \text{ nm}$  were taken successively at a fixed tunnel current ( $3 \text{ nA}$ ). Bottom row: Vector plot of the spin polarization, as obtained from the data shown in the upper rows. Four  $p(2 \times 2)$  unit cells are shown. The color wheel gives the direction and relative magnitude (increasing radially) of the spin polarization. The  $p(2 \times 2)$  (large green square) and  $c(2 \times 2)$  (small green square) cells are marked. Arrows give the direction and relative size of the spin polarization of Mn1, Mn2, Ni1, and Ni2.

terns to form a vector map of the in-plane spin polarization [12]. A map at a given voltage is obtained by adding vectorially a  $90^\circ$ -rotated image of domain 1 to the related image of domain 2. The results show that both the direction and relative magnitude of the spin polarization depend strongly on the bias voltage (bottom row of Fig. 3). At  $-0.1$  V, the contrast between Ni and Mn atoms is weak. The spin polarizations of Mn1 and Mn2 (Ni1 and Ni2) in the  $p(2 \times 2)$  cell both point along  $[010]$  ( $[0\bar{1}0]$ ) but have different magnitudes. At positive bias voltages, strong contrast is present, with spin polarizations of Mn and Ni closely along  $[110]$  and  $[\bar{1}\bar{1}0]$ , respectively. Hence, the spin polarization is rotated by  $45^\circ$  with respect to its  $-0.1$  V orientation.

To summarize the findings obtained so far, the NiMn surface shows an in-plane compensated spin density which is noncollinear in both the space and the energy domain. Even within a single atom, the spin density is noncollinear as a function of the electron energy. This was probed by varying the applied bias voltage which opens the “energy window of tunneling.” Because the spin polarization of the density of states changes with energy, so does the spin polarization of the tunnel current.

Symmetry arguments suggest that the ground-state spin structure of an ideal (unreconstructed) NiMn surface is collinear. However, since there is evidence for reconstruction (from the LEED-IV analysis, Fig. 1), the geometric symmetry is broken, and a noncollinear magnetic structure might evolve. This mechanism requires spin-orbit interaction as a means to couple the orbital degrees of freedom (which are sensitive to the atomic displacements) to the spin degrees of freedom (which determine the spin polarization of the tunnel current).

To support the above explanation of noncollinearity by reconstruction, scalar-relativistic and fully relativistic first-principles electronic-structure calculations were carried out for 6 ML-NiMn films on Cu(001) within the local spin-density approximation to density-functional theory, using Korringa-Kohn-Rostoker methods for layered systems [16,17]. Both the unreconstructed and the experimental geometries were considered in the self-consistent calculations.

For NiMn bulk, the collinear antiferromagnetic phase is energetically preferred to the ferromagnetic phase, in agreement with earlier work [8,9] and calculations for a similar system [NiMn/Ni(001)] [18,19]. The magnetic moments of nearest-neighbor Mn atoms in the film couple antiferromagnetically, whereas those of second-nearest Mn atoms couple ferromagnetically. For the film, the total energy of the reconstructed  $p(2 \times 2)$  cell (with atomic positions taken from the LEED-IV analysis) is lower than that of the ideal  $c(2 \times 2)$  cell, thus supporting the LEED-IV analysis. The surface magnetic moments are  $3.69 \mu_B$  (Mn1),  $3.91 \mu_B$  (Mn2),  $0.30 \mu_B$  (Ni1), and  $0.08 \mu_B$  (Ni2). In contrast to NiMn bulk, the surface Ni atoms have a nonzero magnetic moment. The atom- and spin-resolved density of states of the surface layer (not shown) supports the general

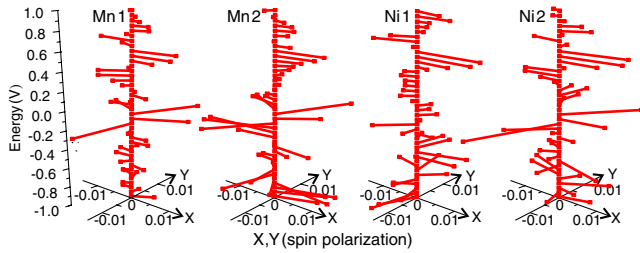


FIG. 4 (color online). Theoretical spin polarization of Mn1, Mn2, Ni1, and Ni2 atoms as a function of energy (Fermi energy at 0 eV). The  $x$  axis ( $y$  axis) is parallel (perpendicular) to Mn sheets. The horizontal spikes visualize direction and size of the in-plane spin polarization, thus indicating a twisting spin polarization in the energy domain.

trend of the spin contrast in STM: weak contrast for negative bias voltages, large for positive bias voltages in agreement with a small (sizable) spin polarization below (above) the Fermi energy.

Calculations of the magnetocrystalline anisotropy for homogeneously magnetized 6 ML films evidence perpendicular anisotropy (energy gain of 3.078 meV per 2D unit cell with respect to the in-plane in-sheet alignment). This corroborates the absence of the layerwise contrast in the experiments since the ring electrode has in-plane spin-sensitive direction. Further, the energy gain for in-plane magnetic moments normal to the Mn (Ni) atomic sheets is 2.651 meV per 2D unit cell. Hence, the magnetization may tilt off the Mn (Ni) sheets easily, in agreement with the experiments but contrary to the bulk case.

To mimic the wave vector filtering by the STM tip, the Bloch spectral function was investigated at  $\vec{k}_{\parallel} = \vec{0}$ . At the center of the Brillouin zone, the local density of states decays slowest towards the vacuum and contributes presumably largest to the tunnel current [20]. By assuming the magnetization perpendicular to the surface, it is found that, without relaxation or without spin-orbit interaction, the spin polarization  $\vec{P}$  of the surface atoms is fully aligned with the magnetization direction, thus forming a collinear spin structure. By taking into account both spin-orbit interaction and relaxation, both the size and direction of the in-plane components of the spin polarization are nonzero and depend significantly on energy (cf. Fig. 4). This indicates an energy-dependent rotation of  $\vec{P}$  associated with each individual atom (Mn1, Mn2, Ni1, and Ni2). Hence, theory supports the explanation of the noncollinear spin patterns found in experiment by reconstruction in interplay with spin-orbit coupling.

In conclusion, the surface spin polarization of the antiferromagnetic alloy NiMn was investigated with atomic resolution. The spin polarization, as obtained by spin-polarized scanning tunneling microscopy, deviates significantly from an expected collinear alignment. This effect is attributed to the interplay of surface reconstruction, i.e., to symmetry breaking within the surface layer, and spin-orbit coupling. This explanation is corroborated by theoretical

densities of states and spectral densities, showing qualitative agreement with respect to the energy dependence of the experimental spin contrast in Sp-STM.

One might speculate that our findings show up also at surfaces of other antiferromagnetic alloys, indicating a possibly general behavior in complex antiferromagnetic materials. The effect may also be present at antiferromagnet-ferromagnet interfaces. The symmetry breaking of the interface structure might then be caused by the relaxation of a lattice mismatch at the interface in the form of a coincidence structure, dislocations, or grain boundaries. In that case, the noncollinear configuration in the real space and the energy domain leads to alterations of the Heisenberg exchange across the interface and could reduce the exchange bias.

- 
- [1] G. A. Prinz, *Science* **282**, 1660 (1998).
  - [2] S. Heinze, M. Bode, A. Kubetzka, O. Pietzsch, X. Nie, S. Blügel, and R. Wiesendanger, *Science* **288**, 1805 (2000).
  - [3] U. Schlickum, N. Janke-Gilman, W. Wulfhchel, and J. Kirschner, *Phys. Rev. Lett.* **92**, 107203 (2004).
  - [4] W. Kuch, L. I. Chelaru, F. Offi, J. Wang, M. Kotsugi, and J. Kirschner, *Nat. Mater.* **5**, 128 (2006).
  - [5] S. van Dijken, M. Besnier, J. Moritz, and J. M. D. Coey, *J. Appl. Phys.* **97**, 10K114 (2005).
  - [6] M. F. Toney, M. G. Samant, T. Lin, and D. Mauri, *Appl. Phys. Lett.* **81**, 4565 (2002).
  - [7] P. M. Oppeneer, H.-C. Mertins, D. Abramsohn, A. Gaupp, W. Gudat, J. Kuneš, and C. M. Schneider, *Phys. Rev. B* **67**, 052401 (2003).
  - [8] J. S. Kasper and J. S. Kouvel, *J. Phys. Chem. Solids* **11**, 231 (1959).
  - [9] E. Krén, E. Nagy, I. Nagy, L. Pál, and P. Szabó, *J. Phys. Chem. Solids* **29**, 101 (1968).
  - [10] C. Tieg, W. Kuch, S. G. Wang, and J. Kirschner, *Phys. Rev. B* **74**, 094420 (2006).
  - [11] U. Schlickum, W. Wulfhchel, and J. Kirschner, *Appl. Phys. Lett.* **83**, 2016 (2003).
  - [12] C. L. Gao, U. Schlickum, W. Wulfhchel, and J. Kirschner, *Phys. Rev. Lett.* **98**, 107203 (2007).
  - [13] W. Wulfhchel and J. Kirschner, *Annu. Rev. Mater. Res.* **37**, 69 (2007).
  - [14] A. Barbieri and M. A. van Hove (private communication); <http://www.sitp.lbl.gov>.
  - [15] J. B. Pendry, *J. Phys. C* **13**, 937 (1980).
  - [16] M. Lüders, A. Ernst, W. M. Temmerman, Z. Szotek, and P. J. Durham, *J. Phys. Condens. Matter* **13**, 8587 (2001).
  - [17] J. Henk, H. Mirhosseini, P. Bose, K. Saha, N. Fomynikh, T. Scheunemann, S. V. Halilov, E. Tamura, and R. Feder, OMN2K-Fully relativistic electron spectroscopy calculations, 2007; the computer code is available from the authors.
  - [18] A. Sakuma, *J. Magn. Mater.* **187**, 105 (1998).
  - [19] D. Spišák and J. Hafner, *J. Phys. Condens. Matter* **11**, 6359 (1999).
  - [20] M. Ondráček, F. Máca, J. Kudrnovský, J. Redinger, A. Biedermann, C. Fritscher, M. Schmid, and P. Varga, *Phys. Rev. B* **74**, 235437 (2006).